Resolving the mystery of milliwatt-threshold opto-mechanical self-oscillation in dual-nanoweb fiber

J. R. Koehler, R. E. Noskov, A. A. Sukhorukov, A. Butsch, D. Novoa, and P. St. J. Russell

Citation: APL Photonics **1**, 056101 (2016); doi: 10.1063/1.4953373
View online: http://dx.doi.org/10.1063/1.4953373
View Table of Contents: http://aip.scitation.org/toc/app/1/5
Published by the American Institute of Physics

Resolving the mystery of milliwatt-threshold opto-mechanical self-oscillation in dual-nanoweb fiber

J. R. Koehler,[1,a] R. E. Noskov,[1] A. A. Sukhorukov,[1,2] A. Butsch,[1,b] D. Novoa,[1] and P. St. J. Russell[1]
[1]*Max-Planck Institute for the Science of Light, Guenther-Scharowsky-Str. 1, 91058 Erlangen, Germany*
[2]*Nonlinear Physics Centre, Research School of Physics and Engineering, Australian National University, Canberra, ACT 2601, Australia*

(Received 22 April 2016; accepted 25 May 2016; published online 28 June 2016)

It is interesting to pose the question: How best to design an optomechanical device, with no electronics, optical cavity, or laser gain, that will self-oscillate when pumped in a single pass with only a few mW of single-frequency laser power? One might begin with a mechanically resonant and highly compliant system offering very high optomechanical gain. Such a system, when pumped by single-frequency light, might self-oscillate at its resonant frequency. It is well-known, however, that this will occur only if the group velocity dispersion of the light is high enough so that phonons causing pump-to-Stokes conversion are sufficiently dissimilar to those causing pump-to-anti-Stokes conversion. Recently it was reported that two light-guiding membranes 20 μm wide, ~500 nm thick and spaced by ~500 nm, suspended inside a glass fiber capillary, oscillated spontaneously at its mechanical resonant frequency (~6 MHz) when pumped with only a few mW of single-frequency light. This was surprising, since perfect Raman gain suppression would be expected. In detailed measurements, using an interferometric side-probing technique capable of resolving nanoweb movements as small as 10 pm, we map out the vibrations along the fiber and show that stimulated intermodal scattering to a higher-order optical mode frustrates gain suppression, permitting the structure to self-oscillate. A detailed theoretical analysis confirms this picture. This novel mechanism makes possible the design of single-pass optomechanical oscillators that require only a few mW of optical power, no electronics nor any optical resonator. The design could also be implemented in silicon or any other suitable material. [http://dx.doi.org/10.1063/1.4953373]

I. INTRODUCTION

The intriguing dynamics of light-sound interactions have been attracting increasing attention due to remarkable advances in experimental techniques, and a wide range of potential applications are emerging.[1] Tight confinement of both photons and phonons, achieved by engineering waveguides and cavities at the nanoscale, reveals a rich landscape of novel optoacoustic phenomena.[2] Key examples include strong enhancement of stimulated Brillouin scattering in silica[3–5] and silicon[6–8] nanowires, spontaneous Brillouin cooling,[9] and on-chip stimulated Brillouin scattering.[10–12]

Whereas in these cases light scatters from propagating acoustic waves, a fundamentally different situation emerges if the driven vibrational resonance is almost entirely transverse: the frequency spacing of the sidebands does not change anymore with the pump frequency so that the optoacoustic interaction closely resembles Raman scattering by molecules. This means that the frequency-wavevector

[a]Author to whom correspondence should be addressed. Electronic mail: johannes.koehler@mpl.mpg.de
[b]Alumna

diagram of the associated phonon is very flat, i.e., its wavevector can be freely chosen while keeping its frequency fixed. For this reason this phenomenon is referred to as stimulated Raman-like scattering (SRLS).[13] It has been observed in a photonic crystal fiber with a solid core ∼1 μm in diameter and a vibrational frequency of a few GHz,[13] and also in a dual-nanoweb fiber structure with very strong optomechanical nonlinearity and a resonant frequency of ∼6 MHz.[14] Recently we reported mechanical self-oscillation of such a dual-nanoweb system when pumped by a few mW of narrow-line single-frequency laser light.[15] This came as a surprise, partly because in previous experiments a dual-frequency pump had always been needed to obtain oscillation, but also for a more subtle reason: Raman gain suppression. Since 1964 it has been known that the Raman gain in a system pumped by a single-frequency laser will be fully suppressed if the pump-to-Stokes and pump-to-anti-Stokes transitions are mediated by phonons of exactly the same frequency and momentum.[16,17] Under these conditions, a phonon created by pump-to-Stokes scattering is immediately annihilated by pump-to-anti-Stokes scattering, which prevents the build-up of the phonon population and suppresses the Raman gain. This phenomenon has been observed under special conditions in bulk gas cells[18] and more recently in hydrogen-filled hollow core photonic crystal fiber.[19]

In the majority of practical cases, however, optical group velocity dispersion causes the pump-to-Stokes and pump-to-anti-Stokes phonons to differ, frustrating gain suppression and leading to strong amplification of the Stokes band above a certain threshold power. In dual-nanoweb fiber, however, almost perfect gain suppression is expected. To understand why this is so, consider a system with group velocity dispersion $\beta_2 = 500$ ps^2/km and a SRLS frequency shift of 6 MHz. For these parameters the dephasing length between pump/Stokes and anti-Stokes/pump phonons $\pi/|\beta_{AS} + \beta_S - 2\beta_P| = \pi/(\beta_2\Omega^2)$ is $\sim 10^9$ m, enormously greater than the ∼10 cm long dual-nanoweb samples. This means that the phonons are essentially identical. Hence the mystery: how can such a system self-oscillate if the SRLS optomechnical gain is strongly suppressed?

In this paper we report a series of detailed measurements, based on a unique interferometric side-probing technique, that, backed by a theoretical model, unwraps the mystery. In brief, gain suppression is unbalanced by the presence of an associated but qualitatively different effect: stimulated intermodal scattering (SIMS) between different guided optical modes of the dual-nanoweb structure. SIMS is related to stimulated interpolarization scattering between orthogonally polarized modes in linearly birefringent fibers[20] and to optoacoustic scattering between counter-propagating Bloch modes in fiber Bragg gratings.[21] It requires a larger amount of phonon momentum than SRLS, and the differing dispersion of the two optical modes means that the acoustic frequency-wavevector relationship is no longer flat, i.e., the phonon frequency depends significantly on its momentum. As a result the frequency shift in SIMS scales with the pump laser frequency, a feature it shares with conventional backward Brillouin scattering.

In order to unbalance SRLS gain suppression, two special conditions must be fulfilled: the SIMS phonon must phasematch SIMS at the same vibrational frequency as SRLS, and a fraction of the pump power must be launched into the higher order fast (f) optical mode in addition to the fundamental slow (s) mode. If this occurs, forward-propagating SIMS phonons would be created by $s \rightarrow f$ transitions from pump to first Stokes which would then be annihilated by $f \rightarrow s$ transitions seeded by pump photons unavoidably launched into the fast mode (Fig. 1(a)). Thus, a cascade of two inter-modal scattering events frustrates gain suppression for SRLS, allowing access to the very large SRLS gain and permitting the system to self-oscillate, generating a large number of side-bands (Fig. 1(b)).

Note that SIMS can also be mediated by backward-propagating phonons created by $f \rightarrow s$ transitions (Fig. 1(b)). Although contributing to the dynamics of the unbalanced system, backward phonons are not capable of unbalancing SRLS gain suppression themselves as only a relatively small fraction of pump power is launched into the fast optical mode in a typical experimental situation. In practice, however, it is impossible to unbalance gain suppression if only one acoustic resonance exists in the system, as is the case in a dual-nanoweb structure that is perfectly symmetric normal to the membrane planes, because the frequencies of SIMS and SRLS cannot coincide (for a structure with two identical membranes 500 nm thick and 22 μm wide they are separated by ∼200 kHz). In an axially uniform structure with upper and lower nanowebs of different thicknesses; however, it is possible to meet this condition via SRLS for the higher-frequency acoustic resonance

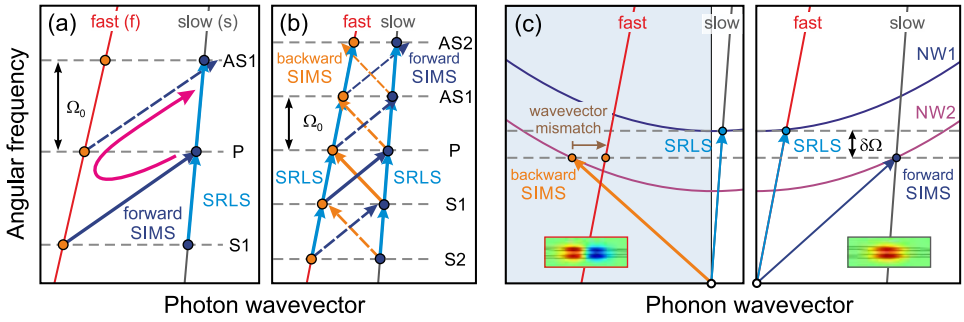

FIG. 1. (a) Dispersion diagram of fast and slow optical modes shows unbalancing of SRLS gain suppression by forward stimulated intermodal scattering (SIMS), leading to self-oscillation for zero frequency detuning between SRLS and SIMS ($\delta\Omega = 0$): $s \rightarrow f$ transitions from pump to 1st Stokes generate forward SIMS phonons which stimulate $f \rightarrow s$ transitions from pump to 1st anti-Stokes. (b) Interplay of SRLS, backward and forward SIMS for $\delta\Omega = 0$ results in the generation of many optical sidebands and self-oscillation. Note that the phonon dephasing for higher order Stokes and anti-Stokes generation, indicated by dashed arrows, is greatly exaggerated in the figure; in the experimental system it is very small (see text). (c) Schematic of the frequency-wavevector diagram for phonons guided in the two nanowebs (NW1 and NW2, each with different cut-off frequencies). The point of zero phonon frequency and wavevector is marked with an open circle, and the dispersion curves of the fast and slow optical modes are also included (simulated field distributions shown as insets). The diagrams show both SRLS and SIMS in forward (left) and backward (right) directions. In the case illustrated, the frequencies for SRLS and SIMS differ by $\delta\Omega$.

and SIMS for the lower frequency resonance, by tuning the laser wavelength so that the frequency detuning $\delta\Omega$ between SRLS and SIMS vanishes (see Fig. 1(c)).

In our case, however, this is achieved even more easily, because the fabricated fibers have significant transverse asymmetries, offering two acoustic resonances, one for each nanoweb, as well as significant axial non-uniformities, permitting frustration of gain suppression at one or more positions along the fiber. As a result self-oscillation is observed at remarkably low powers (a few mW[15]). As we shall see, experimental observations, made by scanning the side-probing beam (Fig. 2) along the fiber, provide convincing evidence for this SIMS/SRLS mechanism of self-oscillation.

II. EXPERIMENTAL SETUP AND DATA ANALYSIS

The fiber used in the experiments (Fig. 2) consists of a capillary supporting two optically coupled nanowebs of width $w \sim 22$ μm. The thicknesses of the upper and lower nanowebs are $h_1 \sim 460$ nm and $h_2 \sim 480$ nm at the center of the fiber, separated by a gap of thickness $h_g \sim 550$ nm. Each web has

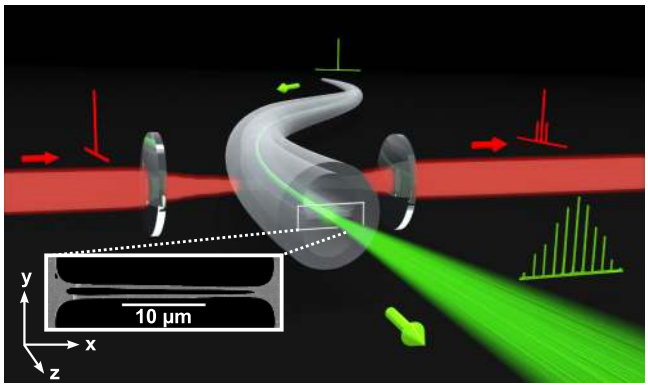

FIG. 2. Sketch of the transverse probing scheme: the green beam represents axially propagating infrared pump light, driving flexural nanoweb resonances, whereas the red beam denotes the transversely launched visible probe light. Inset: scanning electron micrograph of the ~22-μm-wide dual-nanoweb waveguide region. The upper and lower nanowebs are ~460 and ~480 nm thick in the center, spaced apart by ~550 nm.

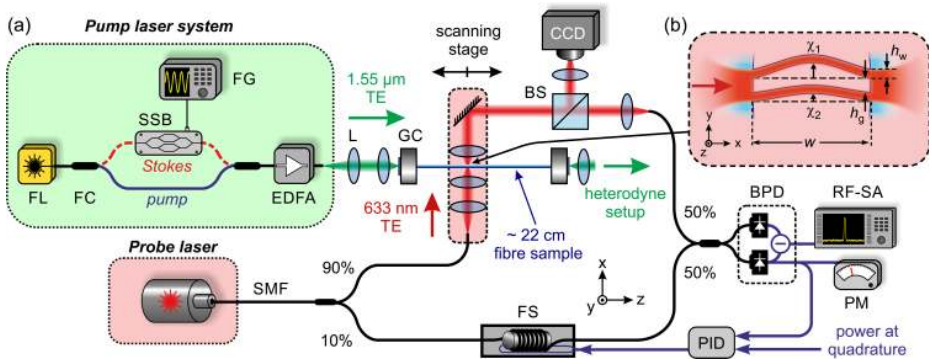

FIG. 3. Mach-Zehnder interferometer setup for transverse probing of flexural resonances in evacuated dual-nanoweb fiber. L: lens, GC: gas cell, BS: beam splitter, CCD: camera, FS: fiber stretcher, SMF: single-mode fiber, BPD: balanced photodiode, PID: proportional-integral-differential controller, RF-SA: RF spectrum analyzer, PM: power meter. (a) The pump laser system at 1550 nm consists of FL: fiber laser, FC: fiber coupler, EDFA: erbium-doped fiber amplifier. Optional (for dual-frequency pumping): SSB: single-sideband modulator, FG: RF function generator. (b) Scheme for transverse probing of the fundamental flexural resonance of the nanowebs. For an idealized structure w is the nanoweb width, h_w the thickness, h_g the gap between the undeflected nanowebs, and χ_1 and χ_2 are their peak deflection amplitudes.

a slightly convex thickness profile, resulting in the formation of bound optical modes. To suppress air-related viscous damping of the mechanical vibrations, each end of the 22-cm-long sample was mounted in a windowed gas cell and the system evacuated to a pressure of ~1 μbar.[22]

Single-frequency pump light at 1550 nm was launched in transverse-electric (TE) polarization into the dual-nanoweb fiber so as to excite mainly the slow (single-lobed) optical mode with a small fraction of the power in the fast (double-lobed) optical mode. The mechanical vibrations were probed by launching a 633 nm HeNe laser beam transversely into the nanowebs through the fiber cladding and monitoring the phase of the transmitted light using a Mach-Zehnder (MZ) interferometer (Fig. 3(a)). To compensate for environmental perturbations while providing high phase sensitivity of the interferometer, the relative optical phase between sample and reference arm was stabilized at $\pi/2$ with a fiber stretcher (FS) driven by a proportional-integral-differential (PID) controller. The intensity-modulated light at the output arms of the MZ was detected using a balanced photodiode (BPD), and the radio-frequency (RF) power spectrum of the BPD current was monitored using an RF spectrum analyzer (RF-SA) with signal-to-noise ratios as high as 33 dB for the strongest signals. The side-probing setup was mounted on a translation stage, allowing the frequencies and amplitudes of the nanoweb vibrations to be mapped out in computer-controlled steps over a fiber length of ~11 cm. Mechanical vibrations with amplitudes as small as 10 pm (see analysis below) could be resolved with an axial resolution of 5 μm, limited by the NA of the focused probe beam. The optomechanical frequency response of the nanowebs at each point was measured by scanning the beat-note of a dual-frequency 1550 nm pump laser and measuring the resulting mechanical motion. The RF spectrum of the transmitted single- and dual-frequency pump light was monitored using a heterodyne technique.[15] The amplitude of the phase modulation in the MZ sample arm can be related to the RF power measured at the MZ output by

$$\varphi(z,\Omega) = 2R^{-1}\sqrt{P_{\mathrm{RF}}(z,\Omega)/\left(8ZP_{\mathrm{sig}}P_{\mathrm{ref}}\right)}, \tag{1}$$

where $\varphi(z,\Omega)$ is the phase-modulation amplitude at the acoustic driving frequency Ω, $P_{\mathrm{RF}}(z,\Omega)$ the RF power measured at the MZ output, R the BPD responsivity in A/W, Z the impedance of the RF-SA, P_{ref} the power in the MZ reference arm, and $P_{\mathrm{sig}}(z)$ the phase-modulated signal. Typical power levels were ~30 μW in the signal and ~90 μW in the reference arms, and away from any flexural resonance the noise level measured by the RF-SA was ~15 fW, leading from Eq. (1) to a minimum detectable phase-modulation amplitude of ~3 μrad.

The change in phase accumulated by the probe light may be calculated as (Fig. 3(b))

$$\varphi(z) = \frac{2\pi}{\lambda}\int_{-w/2}^{w/2}\frac{\partial n_m}{\partial\delta}\delta(x,z)\,dx = \frac{2\pi}{\lambda}\int_{-w/2}^{w/2}\frac{\partial n_m}{\partial\delta}\left(\chi_1(z)\,\hat{\delta}_1(x) - \chi_2(z)\,\hat{\delta}_2(x)\right)dx, \tag{2}$$

where $\lambda = 633$ nm, $n_m(x,z)$ is the local modal index in the nanowebs for the probe light and δ the amount by which the nanowebs deflect towards each other. The function $\hat{\delta}_j(x)$ is the dimensionless flexural mode shape (normalized to its peak value) and $\chi_j(z)$ is the peak deflection of nanoweb j. Numerical modeling yields $\partial n_m/\partial\delta \approx 0.021\ \mu\text{m}^{-1}$ for the idealized structure in Fig. 3(b), allowing us to derive from Eq. (2) the relationship between measured phase modulation and effective peak deflection amplitude χ_{eff}

$$\varphi(z) \approx c_{\text{cal}}(\chi_1 - \chi_2) = c_{\text{cal}}\chi_{\text{eff}}, \tag{3}$$

where $c_{\text{cal}} = 0.253\ \text{rad}/\mu\text{m}$. Although vibrations of both nanowebs play a role in Eq. (3), in practice the individual webs can be clearly distinguished because their resonant frequencies differ. The minimum flexural amplitude that could be resolved in the setup was ~10 pm.

III. IMAGING THE VIBRATIONS: SELF-OSCILLATION

For single-frequency pump powers below the threshold for self-oscillation, very weak thermally driven spontaneous Stokes and anti-Stokes signals at ±5.61 MHz were detected in the transmitted pump light. The estimated effective deflection χ_{eff} in this case is <10 pm, which is below the detection limit of the side-probing system.

At a pump power of 22 mW, above the threshold for self-oscillation, the transmitted RF spectrum shows Stokes and anti-Stokes sidebands up to 5th order with a comb spacing of 5.611 MHz (Fig. 4). The results of a series of side-probe measurements of χ_{eff} are plotted in Fig. 5(a) versus frequency and position along the fiber. The 5.611 MHz flexural resonance first appears at the 22 mm point, remaining detectable from this point onwards. Its resonant frequency is found to vary over a ~3 kHz range, which we attribute to structural non-uniformities.

In Fig. 5(b) χ_{eff} is plotted as a series of data-points, the standard deviations being shown as error bars (each data-point is the result of the root-mean-square average of seven measurements). We attribute these deviations to imperfect interferometer stabilization and seeding of the self-oscillation by thermal phonons. The theoretically calculated contributions from SIMS and SRLS phonons are shown as colored solid curves (see Section VI). By comparing theory with experiment, the 0.15 nm peak deflection at 34 mm can be directly attributed to a SIMS phonon (blue line), whereas the

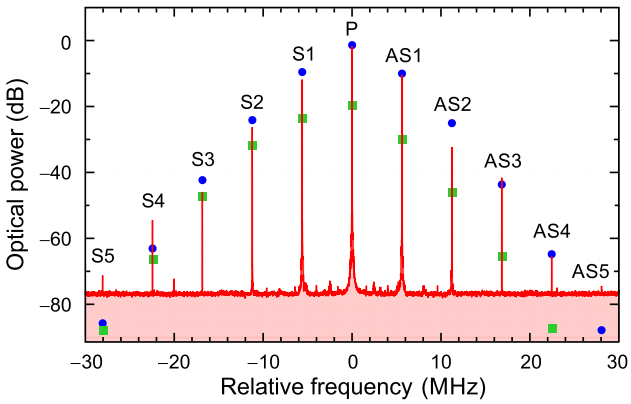

FIG. 4. The solid red line shows the normalized heterodyne spectrum of the optical frequency comb, spaced by 5.611 MHz and generated in transmission through an evacuated dual-nanoweb fiber for 22 mW launched optical power. Up to five orders of Stokes and anti-Stokes lines are observed within a dynamic range of ~75 dB. The blue circles and green squares mark, respectively, the normalized output powers in the slow-mode and fast-mode comb-lines, calculated using the theoretical model in Section VI.

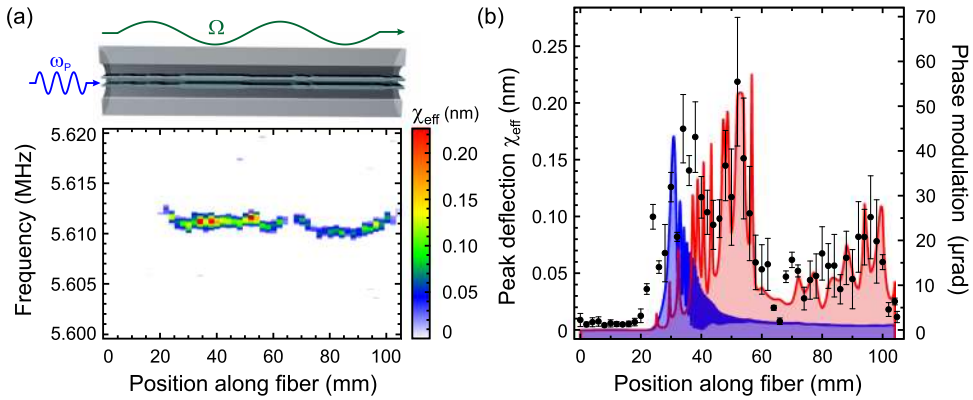

FIG. 5. (a) Measured peak deflection amplitude χ_{eff} plotted as a function of vibrational frequency and position along the fiber for single-frequency pump light. (b) Phase-modulation and deflection amplitude for the flexural resonance at 5.611 MHz as a function of position along the fiber. The error-bars represent the standard deviation calculated from 7 measurements taken at each position. The theoretical model (Section VI) allows the contributions to χ_{eff} from forward SIMS (blue) and SRLS (red) phonons to be distinguished.

0.18 nm peak at 52 mm originates from a SRLS phonon (red line). To estimate the lifetime of the SRLS phonons, we set the probe position to 50 mm and performed a ring-down measurement by recording a time-trace of the RF power decay at 5.611 MHz after switching off the pump light. The decay time was ~0.2 ms, corresponding to a Lorentzian linewidth of $\sim 2\pi \times 400$ Hz.

IV. IMAGING THE VIBRATIONS: DUAL-FREQUENCY EXCITATION

To provide a comprehensive picture of all the optically driven mechanical oscillations, the system was driven by dual-frequency pump light. By sweeping the beat-note frequency while

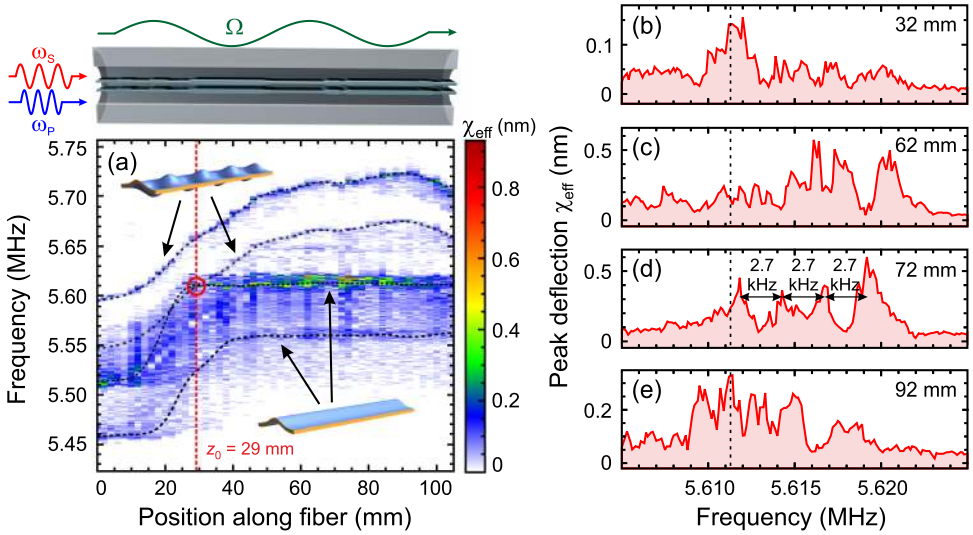

FIG. 6. (a) Transversely probed nanoweb deflection amplitude χ_{eff} as a function of RF drive frequency and position along the fiber for ~18 mW of dual-frequency power. The dashed black lines mark the frequencies of SRLS and SIMS phonons in each nanoweb, the dashed red vertical line shows the position (at 29 mm) where the SRLS and SIMS frequencies coincide. (b)–(e) Peak nanoweb deflection amplitude χ_{eff} of the comb-generating flexural resonance as a function of drive frequency at 32, 62, 72, and 92 mm along the fiber. Strong inhomogeneous broadening is observed, caused by structural non-uniformities. The vertical dashed line marks the comb-spacing measured when the system is driven into self-oscillation by a single-frequency pump.

probing the vibrations at each position along the fiber, the spatial distribution and strength of all the optically-driven flexural vibrations could be measured. Figure 6(a) shows a detailed spatial and frequency map of the nanoweb deflection as a function of drive laser beat-frequency and position along the fiber. The largest deflection occurs at 5.611 MHz in the region between 24 and 104 mm, in good agreement with the parameters measured for the SRLS phonon under single-frequency pumping (Sec. III). For a total dual-frequency pump power of 18 mW, the measured χ_{eff} (which occurred at 74 mm) was 0.9 nm, compared to ~0.2 nm for single-frequency pumping with 22 mW. Within the same fiber section a second resonance is seen to follow a parallel trajectory at an ~53 kHz lower frequency (~5.56 MHz). We attribute this to SRLS phonons in the second nanoweb. Figure 6(a) reveals two further resonances at higher frequency (the upper of these runs from 5.59 to 5.73 MHz) that follow parallel trajectories along the whole fiber length with a spacing of ~47 kHz. The peak deflection amplitudes are ~0.1 nm for the lower and ~0.3 nm for the higher-frequency resonance. We attribute these to SIMS phonons in each nanoweb. The lifetime of these phonons was next measured by ring-down at the 50 mm point. With the dual-frequency beat-note tuned to 5.70 MHz, the pump light was abruptly switched off. The decay time of the RF signal was ~0.1 ms, corresponding to a linewidth of $\sim 2\pi \times 800$ Hz.

The frequencies of both SIMS phonons reach local maxima at 87 mm, altering over a range of ±7 mm by less than the mechanical linewidth. Consequently, when the dual-frequency beat-note is fixed at 5.72 MHz, power transfer from the pump to the first-order Stokes sideband can only be achieved by a single SIMS transition over a nonlinear interaction length of ~14 mm. This allowed us to estimate the SIMS gain by launching a weak seed signal at the first Stokes frequency and measuring the amplification factor as a function of single-frequency pump power. The resulting value of ~0.06 μm^{-1} W^{-1} agrees well with the theoretical estimate in Section VI.

Fig. 6(a) shows that the frequencies of SIMS and SRLS coincide at 5.611 MHz and ~29 mm, which is the point at which SIMS is able to frustrate SRLS gain suppression. Figs. 6(b)-6(e) show a series of high resolution measurements at z = 32, 62, 72, and 92 mm, taken over the frequency range 5.615 ± 0.01 MHz (in the vicinity of the self-oscillating SRLS transition at 5.611 MHz). The nanoweb deflection at 5.611 MHz is noticeably weaker at z = 62 mm, coinciding with the point where the self-oscillation amplitude strongly dropped (Section III). Furthermore, structural non-uniformities cause inhomogeneous broadening of the resonance, which, for example, splits into four sub-peaks spaced a few kHz apart at the 72 mm point.

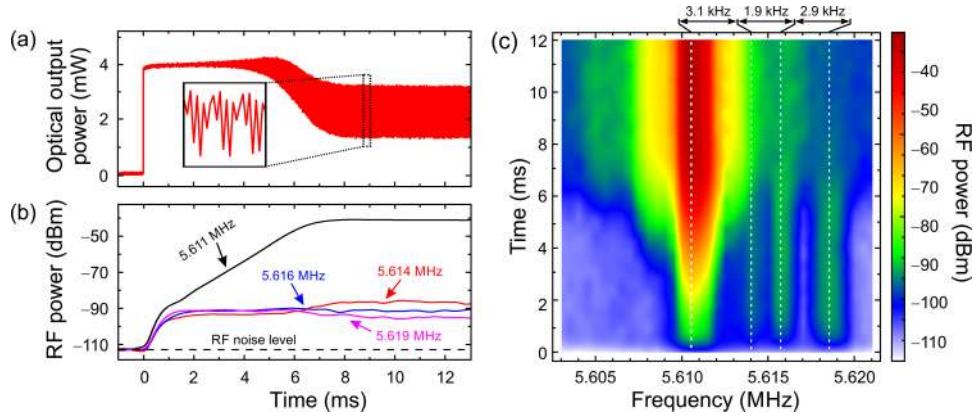

FIG. 7. (a) Time-dependence of the transmitted optical power immediately after switching on the single-frequency pump laser at $t = 0$. The pump power is 22 mW, above the threshold for self-oscillation. The transmitted power drops by ~36% in the steady state, at which point complex beating between the multiple optical sidebands is seen (inset: zoom-in). (b) Time traces of the RF power in the spectral bands at 5.611, 5.614, 5.616, and 5.619 MHz. The signal at 5.611 MHz is amplified, while the growth of other signals is suppressed. (c) Transmitted RF spectrum as a function of time during growth of self-oscillation.

V. DYNAMICS OF SELF-OSCILLATION

By monitoring the RF spectrum of the transmitted pump light, the evolution of these sub-resonances could be followed over time by pumping the system with square-wave-modulated single-frequency light at a peak power level above the threshold for self-oscillation. Each "on" cycle was 40 ms long, which was long enough for the system to reach steady-state.

Fig. 7(a) shows the transmitted optical power collected with a single-mode fiber (SMF) and detected with a photodiode. Roughly 7 ms after initiation of self-oscillation, a steady state is reached. As already explained, self-oscillation is initiated by strong SIMS coupling from the slow to the fast optical mode. Since the fast mode has a higher leakage loss, the result is a 36% drop in average transmitted power.

The time-evolution of the individual resonances at 5.611, 5.614, 5.616, and 5.619 MHz is shown in Fig. 7(b). Over the build-up time of ~7 ms, all four resonances could be detected, with the 5.611 MHz resonance winning out in the competition for gain. This can also be seen in Fig. 7(c), which shows the evolution of the RF spectrum with time.

VI. THEORETICAL MODEL AND DISCUSSION

In this section, we develop a theoretical model of the system. We restrict the analysis to TE-polarized optical modes and fundamental acoustic flexural modes in the nanowebs. Measurements of the spatial distribution of the mechanical vibrations show that the geometrical parameters (width, thickness, interweb spacing, convex profile) vary much more slowly along the fiber than in the transverse direction (the characteristic scale of axial inhomogeneity is ~1 mm (Fig. 6(a)), whereas the nanoweb width is ~22 μm). These considerations lead to the following set of coupled equations valid in the steady-state (see supplementary material[23]):

$$\frac{\alpha_s}{2}s_n + \frac{\partial s_n}{\partial z} = i\frac{\omega_n}{\omega_0}\sum_{j=1}^{2}\left[\kappa^j_{sRs}\left(R_j s_{n-1} + R_j^* s_{n+1}\right) + \kappa^j_{sMf}\left(M_j^+ f_{n-1} + M_j^{-*} f_{n+1}\right)\right], \tag{4a}$$

$$\frac{\alpha_f}{2}f_n + \frac{\partial f_n}{\partial z} = i\frac{\omega_n}{\omega_0}\sum_{j=1}^{2}\left[\kappa^j_{fRf}\left(R_j f_{n-1} + R_j^* f_{n+1}\right) + \kappa^j_{fMs}\left(M_j^+ s_{n-1} + M_j^{-*} s_{n+1}\right)\right], \tag{4b}$$

$$R_j\frac{i\Omega\Gamma_{jR} + \Omega^2 - \Omega^2_{jR}(z)}{2i\Omega} = i\kappa^j_{Rss}\sum_n s_n s^*_{n-1} + i\kappa^j_{Rff}\sum_n f_n f^*_{n-1}, \tag{4c}$$

$$M_j^+\frac{i\Omega\Gamma_{jM} + \Omega^2 - \Omega^2_{jM}(z)}{2i\Omega} + V_{jM}\frac{\partial M_j^+}{\partial z} = i\kappa^j_{Msf}\sum_n s_n f^*_{n-1}, \tag{4d}$$

$$M_j^-\frac{i\Omega\Gamma_{jM} + \Omega^2 - \Omega^2_{jM}(z)}{2i\Omega} - V_{jM}\frac{\partial M_j^-}{\partial z} = i\kappa^j_{Msf}\sum_n s^*_n f_{n+1}. \tag{4e}$$

Here s_n and f_n represent the slowly varying dimensionless field amplitudes of the nth comb lines (negative values correspond to Stokes components) for the slow and fast optical modes, with frequencies $\omega_n = \omega_0 + n\Omega$ and axial propagation constants $\beta_{sn} = \beta_{s0} + nq$ and $\beta_{fn} = \beta_{f0} + nq$, where ω_0 is the optical pump frequency, β_{s0}, β_{f0} the wavevectors, Ω and q the beat-note frequency and propagation constant, and α_s and α_f the loss rates of the launched pump modes. The subscripts R and M represent SRLS and SIMS phonons, R_j and $M_j^{\pm}$ denote their dimensionless slowly varying field envelopes (+ for forward and − for backward phonons), $j = 1,2$ refers to the upper and lower nanoweb, $\Omega_{jR}(z)$ and $\Omega_{jM}(z)$ are the phonon eigenfrequencies, Γ_{jR} and Γ_{jM} their decay rates and V_{jM} is the group velocity of the SIMS phonons (the group velocity of the SRLS phonons is approximately zero). The rates of opto-acoustic coupling for the various transitions are given by $\kappa^j_{\eta\zeta\xi}$ where η, ζ, and ξ are combinations of R, M, s, and f. The derivation of the model, together with detailed definitions of all these parameters is available in the supplementary material.[23]

The SRLS and SIMS wavevectors differ significantly, with values $q_R = \Omega n_s/c \approx 0.14\ \mathrm{m}^{-1}$ and $q_M = (n_s\omega_0 - n_f\,\omega_{-1})/c \approx 54.3\ \mathrm{mm}^{-1}$ for $\Omega = 2\pi \times 5.611$ MHz and modal indices $n_s = 1.2369$ and $n_f = 1.2235$. These translate to acoustic wavelengths of ~45 m (SRLS) and 116 μm (SIMS). The dephasing rate between SIMS transitions in adjacent side-bands is $\Delta q = (n_s - n_f)\Omega/c \sim 1.6\ \mathrm{km}^{-1}$, yielding a characteristic length of ~4 km. Since the fiber length is ~22 cm, the dephasing between adjacent comb-lines can be neglected for both SRLS and SIMS phonons.

The boundary conditions for Eq. (4) can be written as follows:

$$s_n(0) = \sqrt{P_{s0}/P_0}\,\delta_{n,0} + \sqrt{P_{noise}/P_0}\,(\delta_{n,-1} + \delta_{n,+1}),$$
$$f_n(0) = \sqrt{P_{f0}/P_0}\,\delta_{n,0} + \sqrt{P_{noise}/P_0}\,(\delta_{n,-1} + \delta_{n,+1}),\ M_j^+(0) = M_j^-(L) = 0,$$

where $\delta_{n,0(\pm1)}$ is the Kronecker delta, L the fiber length, P_{s0} and P_{f0} the pump powers launched into the slow and fast optical modes ($P_0 = P_{s0} + P_{f0}$), and $P_{noise} = k_B T \Omega_{jR}\Gamma_{jR}/(2\omega_0)$ is the effective input noise power in first-order side-bands[24] where k_B is Boltzmann's constant and T is the temperature. We neglect slight differences in noise power for the SRLS and SIMS transitions. When the backward SIMS phonon is included in Eq. (4e), the boundary conditions are split. To deal with this, an iterative scheme was used in which Eqs. (4a)–(4e) were solved sequentially until convergence was reached.

To explain the origins of gain suppression, we consider pure SRLS in the slow optical mode in an axially homogeneous system (i.e., $P_{f0} = 0$). The equations can then be recasted as follows:

$$\frac{\partial P_s}{\partial z} = -\alpha_s P_s - \sum_j e_j\Gamma_{jR},\ \text{with}\ e_j = \frac{P_0^2\Omega|\Phi_{ss}|^2}{\omega_0\Gamma_{jR}}\,g_j^{ss}(\Omega, z),$$
$$g_j^{ss}(\Omega, z) = g_{0j}^{ss}\frac{(\Gamma_{jR}/2)^2}{(\Omega - \Omega_{jR}(z))^2 + (\Gamma_{jR}/2)^2}, \tag{5}$$

where $P_s = P_0\sum_n |s_n|^2$ is the total optical power in the slow mode, e_j the acoustic energy per unit length in the SRLS phonon in one of the webs, $\Phi_{ss} = \sum_n s_n s_{n-1}^*$ is the strength of the optical beat-note that drives the mechanical vibrations (the "optical force"), and $g_j^{ss}(\Omega, z)$ is the gain spectrum with peak value $g_{0j}^{ss} = 4\kappa_{sRs}^j\kappa_{Rss}^j/(P_0\Gamma_{jR})$ at resonance. The quantity $\sum_j e_j\Gamma_{jR}$ may be viewed as the mechanical work done by the optical field, while we prove that Φ_{ss} only depends on the loss (assuming the coupling constants in Eq. (4) are independent of frequency, i.e., $\omega_n/\omega_0 \approx 1$)

$$\frac{\partial\Phi_{ss}}{\partial z} = -\alpha_s\Phi_{ss}. \tag{6}$$

As a result a curious and rather unique situation emerges: even when the SRLS gain is high, Φ_{ss} is determined solely by the input optical field and the fiber parameters. It cannot increase along the fiber, which implies that it is zero everywhere if $\Phi_{ss}(0) = 0$ (the case for a single-frequency pump). Although under these circumstances the sidebands are seeded by noise, on average $\Phi_{ss}(0)$ will still be zero. If a dual-frequency pump is used, on the other hand, $\Phi_{ss}(0) \neq 0$ and power can be exchanged between the side-bands as the field progresses along the fiber.

The optical force in SIMS interactions is $\Phi_{sf} = \sum_n s_n f_{n-1}^*$, which for $V_{1M} = V_{2M} \sim 0$ satisfies the following equation:

$$\frac{\partial|\Phi_{sf}|^2}{\partial z} = \left[-\alpha_s - \alpha_f + \Delta P(z)\,g_{\mathrm{eff}}^{sf}(\Omega, z)\right]|\Phi_{sf}|^2, \tag{7}$$

where $\Delta P(z) = P_0\sum_n\left[|s_n(z)|^2 - |f_{n-1}(z)|^2\right]$ is the power difference between adjacent comb-lines and $g_{\mathrm{eff}}^{sf}(\Omega, z) = g_1^{sf} + g_2^{sf}$ is the effective SIMS gain. Although for single-frequency pumping $\Phi_{sf}(0) = 0$, the system is able to strongly amplify side-band noise since unlike in SRLS (Eq. (6)) gain is not suppressed.

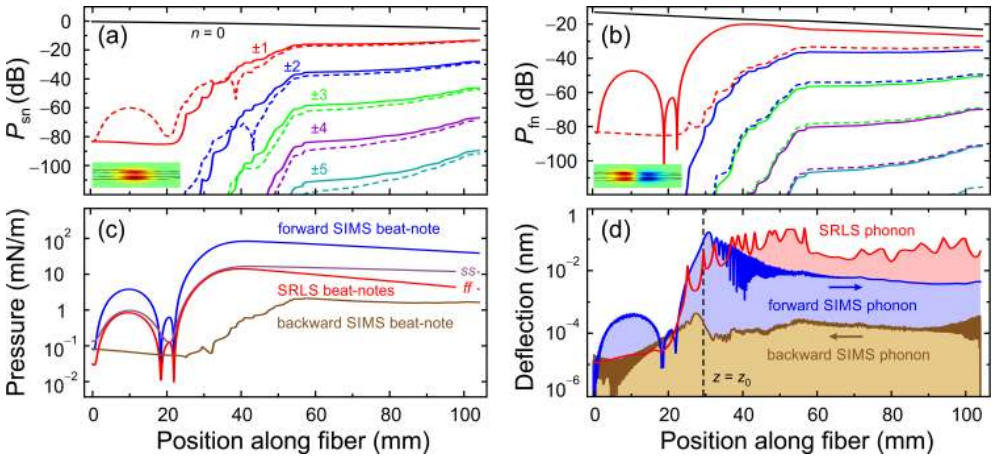

FIG. 8. Spatial evolution of the normalized power in the comb-lines for (a) slow and (b) fast optical modes at $P_0 = 41.5$ mW. The full lines mark the Stokes and the dashed lines mark the anti-Stokes sidebands. The numbers by the curves are the sideband orders. (c) Strength of the optical beat-notes driving the SRLS and SIMS transitions. (d) Spatial distribution of the peak nanoweb deflections for the backward and forward SIMS phonons and the SRLS phonon. The forward SIMS phonon reaches a peak amplitude close to $z_0 = 29$ mm, where it is exactly frequency-matched to the SRLS phonon (see Fig. 6(a)).

To model evolution of comb-line amplitudes, we used the measured spatial dependence of the phonon frequencies (Fig. 6(a)) and set the beat-note frequency equal to the frequency of self-oscillation, i.e., $\Omega/2\pi = 5.611$ MHz. We also set $P_{s0}/P_0 = 0.95$ and $P_{f0}/P_0 = 0.05$: the relative strengths of the fast and slow modes can be adjusted experimentally by varying the focal size and position of the launched pump light. From the experimental parameters we estimated the linewidths ($\Gamma_{jR}/2\pi = 400$ Hz and $\Gamma_{jM}/2\pi = 800$ Hz), optical losses ($\alpha_s = 8.1$ m^{-1} and $\alpha_f = 24.3$ m^{-1}), effective optical noise power ($P_{noise} = 0.2$ nW), and the group velocity of the SIMS phonons ($V_{1M} = V_{2M} = 12$ m/s). For other parameters see the supplementary material.[23] Remarkably high gain factors are predicted by the theory: $g_{0j}^{ss} \approx 0.18\ \mu\text{m}^{-1}\,\text{W}^{-1}$, $g_{0j}^{ff} \approx 0.14\ \mu\text{m}^{-1}\,\text{W}^{-1}$, and $g_{0j}^{sf} \approx 0.053\ \mu\text{m}^{-1}\,\text{W}^{-1}$ at 1550 nm.

Figures 8(a) and 8(b) plot the evolution of the fast-mode and slow-mode sideband power along the fiber for $P_0 = 41.5$ mW. Also plotted is the strength of the optical beat-notes that drive phonon creation (Fig. 8(c)) and the peak nanoweb deflections χ_{eff} (Fig. 8(d)). Close to the fiber input, noise-seeded $s \rightarrow f$ transitions from pump to first Stokes generate forward-propagating SIMS phonons. These phonons then scatter fast-mode pump photons into slow-mode photons at the first anti-Stokes frequency (see Fig. 1(a)). As a result, optical signals with unbalanced sideband powers arrive at $z_0 = 29$ mm, the point where the SRLS and SIMS processes are frequency-matched, resulting in the frustration of gain suppression and access to very high SRLS gain (see Fig. 1(b)). Note that the backward SIMS phonons contribute very little to the inter-modal transitions (Fig. 8(d)) because of relatively weak initial seeding of the fast mode.

The strong effect of the spatial and spectral co-location of SRLS and SIMS is also reflected in the amplitudes of the optical forces and nanoweb vibrations (Figs. 8(c) and 8(d)). In particular, the optical beat-note that drives SIMS shows aperiodic cycling for $z < z_0$, with saturation at $z = z_0$ and subsequent decay by optical losses in accordance with Eq. (7). Remarkably, the SIMS driving term dominates along the whole length of the fiber despite the fact that the SRLS phonon amplitude exceeds the SIMS phonon amplitude. This is because the SIMS beat-note, the strength of which is determined by the large imbalance in side-band amplitudes at $z = z_0$, does not have the correct frequency and wavevector combination to resonantly drive the SIMS phonon for $z > z_0$.

Finally, we point out excellent agreement between the output frequency comb spectra and vibration amplitudes obtained by numerical simulations and experimentally measured, as shown in Figs. 4 and 5(b). The only discrepancy was the single-frequency pump power required: 22 mW in

the experiments compared to 41.5 mW in the modeling. We attribute this to the limited scanning range of the side-probe beam, which made it impossible to characterize the vibrational properties of the sample along its entire length.

VII. CONCLUSIONS

Suppression of giant Raman-like gain in optomechanical systems is expected if the group velocity dispersion is negligible over the device length for the frequency bandwidth considered. This is the case in dual-nanoweb fiber, where the Raman-like resonant frequency is ~6 MHz and the device length ~10 cm. The unexpected observation of self-oscillation at mW single-frequency pump powers, an indication that stimulated Raman-like scattering (SRLS) does indeed occur, is caused by simultaneous excitation, at the same frequency, of SRLS and stimulated intermodal scattering (SIMS), made possible because each web has a different flexural wave cut-off frequency. With the addition of at least a small amount of pump power in the higher order (fast) optical mode, SRLS gain suppression is frustrated and the system goes into self-oscillation above a certain threshold power. The difficulty of fulfilling these special conditions in an axially homogeneous stucture is relaxed in a structure with axial non-uniformities, such as the dual nanoweb fibers discussed here. With more accurate fabrication, such as that offered by silicon photonics, it may be possible to meet these conditions in a sample with negligible axial non-uniformity, perhaps with some small tuning of the pump laser frequency. This could lower the threshold for self-oscillation still further, perhaps to the μW range, while offering oscillation frequencies in the GHz range or even higher.

ACKNOWLEDGMENTS

A.A.S. gratefully acknowledges financial support from the Alexander von Humboldt Foundation and the Australian Research Council (Discovery Project No. DP130100086).

[1] M. Maldovan, "Sound and heat revolutions in phononics," Nature **503**, 209–217 (2013).
[2] P. T. Rakich, C. Reinke, R. Camacho, P. Davids, and Z. Wang, "Giant enhancement of stimulated Brillouin scattering in the subwavelength limit," Phys. Rev. X **2**, 011008 (2012).
[3] P. Dainese, P. St. J. Russell, N. Joly, J. C. Knight, G. S. Wiederhecker, H. L. Fragnito, V. Laude, and A. Khelif, "Stimulated Brillouin scattering from multi-GHz-guided acoustic phonons in nanostructured photonic crystal fibres," Nat. Phys. **2**, 388–392 (2006).
[4] O. Florez, P. F. Jarschel, Y. A. V. Espinel, C. M. B. Cordeiro, T. P. M. Alegre, G. S. Wiederhecker, and P. Dainese, "Brillouin scattering self-cancellation," Nat. Commun. **7**, 11759 (2016).
[5] J.-C. Beugnot, S. Lebrun, G. Pauliat, H. Maillotte, V. Laude, and T. Sylvestre, "Brillouin light scattering from surface acoustic waves in a subwavelength-diameter optical fibre," Nat. Commun. **5**, 5242 (2014).
[6] H. Shin, W. Qiu, R. Jarecki, J. A. Cox, R. H. Olsson, A. Starbuck, Z. Wang, and P. T. Rakich, "Tailorable stimulated Brillouin scattering in nanoscale silicon waveguides," Nat. Commun. **4**, 1944 (2013).
[7] R. Van Laer, A. Bazin, B. Kuyken, R. Baets, and D. Van Thourhout, "Net on-chip Brillouin gain based on suspended silicon nanowires," New J. Phys. **17**, 115005 (2015).
[8] R. Van Laer, B. Kuyken, D. Van Thourhout, and R. Baets, "Interaction between light and highly confined hypersound in a silicon photonic nanowire," Nat. Photonics **9**, 199–203 (2015).
[9] G. Bahl, M. Tomes, F. Marquardt, and T. Carmon, "Observation of spontaneous Brillouin cooling," Nat. Phys. **8**, 203–207 (2012).
[10] H. Shin, J. A. Cox, R. Jarecki, A. Starbuck, Z. Wang, and P. T. Rakich, "Control of coherent information via on-chip photonic–phononic emitter–receivers," Nat. Commun. **6**, 6427 (2015).
[11] M. Merklein, I. V. Kabakova, T. F. S. Büttner, D.-Y. Choi, B. Luther-Davies, S. J. Madden, and B. J. Eggleton, "Enhancing and inhibiting stimulated Brillouin scattering in photonic integrated circuits," Nat. Commun. **6**, 6396 (2015).
[12] R. Pant, C. G. Poulton, D.-Y. Choi, H. Mcfarlane, S. Hile, E. Li, L. Thevenaz, B. Luther-Davies, S. J. Madden, and B. J. Eggleton, "On-chip stimulated Brillouin scattering," Opt. Exp. **19**, 8285–8290 (2011).
[13] M. S. Kang, A. Nazarkin, A. Brenn, and P. St. J. Russell, "Tightly trapped acoustic phonons in photonic crystal fibres as highly nonlinear artificial Raman oscillators," Nat. Phys. **5**, 276–280 (2009).
[14] A. Butsch, M. S. Kang, T. G. Euser, J. R. Koehler, S. Rammler, R. Keding, and P. St. J. Russell, "Optomechanical nonlinearity in dual-nanoweb structure suspended inside capillary fiber," Phys. Rev. Lett. **109**, 183904 (2012).
[15] A. Butsch, J. R. Koehler, R. E. Noskov, and P. St. J. Russell, "CW-pumped single-pass frequency comb generation by resonant optomechanical nonlinearity in dual-nanoweb fiber," Optica **1**, 158–164 (2014).
[16] N. Bloembergen and Y. R. Shen, "Coupling between vibrations and light waves in Raman laser media," Phys. Rev. Lett. **12**, 504 (1964).

[17] Y. R. Shen and N. Bloembergen, "Theory of stimulated Brillouin and Raman scattering," Phys. Rev. **137**, A1787–A1805 (1965).
[18] M. D. Duncan, R. Mahon, J. Reintjes, and L. L. Tankersley, "Parametric Raman gain suppression in D_2 and H_2," Opt. Lett. **11**, 803–805 (1986).
[19] S. T. Bauerschmidt, D. Novoa, and P. St. J. Russell, "Dramatic Raman gain suppression in the vicinity of the zero dispersion point in a gas-filled hollow-core photonic crystal fiber," Phys. Rev. Lett. **115**, 243901 (2015).
[20] M. S. Kang, A. Butsch, and P. St. J. Russell, "Reconfigurable light-driven opto-acoustic isolators in photonic crystal fibre," Nat. Photonics **5**, 549–553 (2011).
[21] W. F. Liu, P. St. J. Russell, and L. Dong, "100% efficient narrow-band acoustooptic tunable reflector using fiber Bragg grating," J. Lightwave Technol. **16**, 2006–2009 (1998).
[22] J. R. Koehler, A. Butsch, T. G. Euser, R. E. Noskov, and P. St. J. Russell, "Effects of squeezed-film damping on the optomechanical nonlinearity in dual-nanoweb fiber," Appl. Phys. Lett. **103**, 221107 (2013).
[23] See supplementary material at http://dx.doi.org/10.1063/1.4953373 for a derivation of coupled Equation (4) governing the evolution of the optical frequency comb.
[24] A. Kobyakov, M. Sauer, and D. Chowdhury, "Stimulated Brillouin scattering in optical fibers," Adv. Opt. Photonics **2**, 1–59 (2010).